2021

Effect of Surface Roughness and External Loading on Embedment in Steel and Aluminum Bolted Joints

Nathan Stang
South Dakota State University

EFFECT OF SURFACE ROUGHNESS AND EXTERNAL LOADING ON EMBEDMENT IN STEEL AND ALUMINUM BOLTED JOINTS

By

NATHAN STANG

A thesis submitted in partial fulfillment of the requirements for the

Master of Science

Major in Mechanical Engineering

South Dakota State University

2021

THESIS ACCEPTANCE PAGE

Nathan Stang

This thesis is approved as a creditable and independent investigation by a candidate for the master's degree and is acceptable for meeting the thesis requirements for this degree. Acceptance of this does not imply that the conclusions reached by the candidate are necessarily the conclusions of the major department.

Todd Letcher
Advisor Date

Kurt Bassett
Department Head Date

Nicole Lounsbery, PhD
Director, Graduate School Date

ACKNOWLEDGEMENTS

This thesis was made possible by the South Dakota State University Mechanical Engineering Department, and my research sponsor Jon Ness from Matrix Engineering. An additional thanks to Dr. Todd Letcher, Thesis Advisor, Dr. Zhong Hu, Graduate Coordinator, and Bryan Romsa, thesis committee member.

CONTENTS

LIST OF FIGURES

LIST OF TABLES

ABSTRACT

EFFECT OF SURFACE ROUGHNESS AND EXTERNAL LOADING ON EMBEDMENT IN STEEL AND ALUMINUM BOLTED JOINTS

2021

Embedment in bolted joints is defined as the local deformation of surfaces into one another due to uneven contact. Embedment that occurs after the tightening of a bolted joint can cause loss of preload in the joint potentially leading to failure. VDI 2230, a German standard for bolted joint design, is currently the main source for engineers regarding embedment. It related expected embedment to the surface roughness in steel bolted joints. This research expands on the VDI standard by performing tests on a commonly used aluminum alloy and a steel alloy. Both cold rolled 1045 steel and 6061-T6511 aluminum bolted joints preload losses were monitored using M10 class 8.8 and 12.9 stain gauge bolts with joint interfaces having varying surface roughness. The joints were loaded to 75% of their proof load, and shear loaded externally in a sine wave using a universal testing machine. The slip coefficient was also found for each surface roughness. Results showed that as surface roughness increases embedment, and the slip coefficient increases. As the external shear load increased the amount of initial embedment increased. At the same external shear load and roughness T6511 aluminum displayed on average 50% more embedment than 1045 cold rolled steel. The results showed that aluminum will embed more than steel at the same preload and shear load, embedment values are affected by external shear force, material surface roughness, and surface slip coefficient. Embedment was also tested with joints having various clamp

lengths and it was determined for the clamp lengths used in this experiment that embedment is not a function of clamp length.

1.0 INTRODUCTION

Bolted joints are used widely in almost all fields related to engineering. It is important for engineers to understand every aspect of bolted joint design when designing critical fasteners. After bolted joints are tightened, one of the ways they can lose clamp load or preload is plastic relaxation or embedment. Embedment is the local deformation of surfaces into one another due to uneven contact. Uneven contacted is caused by imperfections in material surfaces. Figure 1 displays a visual representation of surface imperfections [1]. Most of a bolted joint's embedment occurs initially during bolt tightening, but embedment after tightening can cause unexpected loss of clamp load potentially leading to failure of a bolted joint. This is especially critical for joints with smaller clamp lengths. Embedment occurs between any two interfaces in contact. In bolted joints the nut/bolt head to washer, washer to plate, plate to plate, and nut thread to bolt thread interfaces are all sources of embedment.

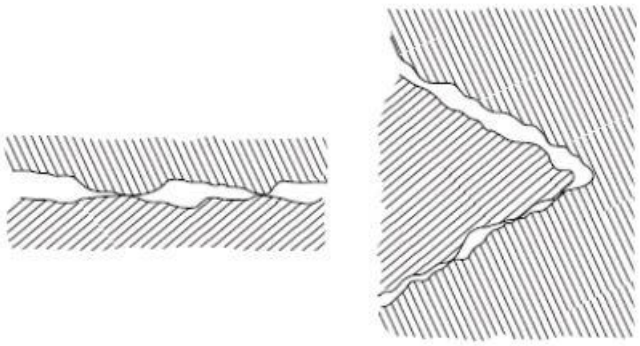

Figure 1: Visualizing imperfection in thread and contact surfaces (Blatt 2003) [1]

This research aims to study embedment in bolted joints of steel and aluminum by relating material roughness to expected embedment and test conclusions made by previous researchers regarding embedment using carbon steel strain gauge bolts. Prior research has been conducted on embedment by Mohamad Ba Saleem [2]. Ba Saleem

experimented with embedment in 1045 steel, and he is currently cited in the VDI 2230 [3]. VDI stands for Verein Deutscher Ingenieure translated to English is the Association of German Engineers and their standard the VDI 2230 is the state-of-the-art reference regarding bolted joint design. Ba Saleem's research related embedment to surfaces roughness by using the surfaces mean roughness depth or Rz value. He also concluded that a joints clamp length does not have any effect on the amount of embedment that occurs in the system. Ba Saleem did not experiment with aluminum, but the VDI cites Lori [4] who concluded that embedment in bolted joints of aluminum in greater, with no numerical quantity.

By equipping bolts with axially inserted strain gauges, much like Ba Saleem, the loss in preload of bolted joints of aluminum and steel bolted joints could be monitored and quantified. The bolts used in this experiment were property class 8.8 and 12.9 DIN-931 [5] M10 x 1.5 x 60 mm. The use of high carbon steel and alloy steel bolts reduces the effects of viscoelasticity. Viscoelasticity is the rate-dependent inelastic behavior of solids, meaning that the deformation of the material depends on the rate at which the load is applied. Viscoelasticity is molecular rearrangement, the time dependent process by which viscoelasticity occurs is commonly referred to as creep. Masayuki Tendo studied viscoelasticity and material creep and noted that high carbon steels experience dynamic strain aging at room temperature [6]. Creep failure is the time-dependent and permanent deformation of a material when subjected to a constant load or stress. It is difficult to distinguish between preload losses due to creep or embedment.

Ba Saleem's conclusion that clamp length does not affect embedment was tested by monitoring bolted joints with various clamp lengths. Control testing was also

performed on aluminum joints with bolted joints having no inner interfaces to isolate the embedment in the inner interfaces from the embedment in the threads and at the bolt head interface. These tests could not be loaded in the UTM, so they were performed statically over three days. The statically tested samples were kept inside of a temperature-controlled water bath as the temperature fluctuation over three days would affect test results. Ba Saleem observed from his static testing that embedment after three days is negligible. He also stated that embedment in static testing did not vary from tests conducted with dynamic external axial loading for 1045 steel, but it is unknown if this phenomenon will be true for aluminum alloys which have been proven to have a higher rate of creep in comparison to carbon steel alloys [6]. The control testing therefore will be more effected by creep then dynamic testing as dynamic testing is conducted over a shorter period. Ba Saleem also concluded that as the roughness of the internal surfaces increased the amount of embedment that occurred in the joint also increased.

2.0 LITERATURE REVIEW

2.1 VDI 2230 5.1.1 Axial Resilience

The design process defined in VDI 2230 standard is the state of art for dynamically loaded bolted joints. The VDI 2230 Part 1, 5.1.1.1 describes the elastic resilience of BJ based on its components and 5.4.2 describes the losses in preload of a bolted joint. The symbols, abbreviations, and figures used in this paper follow the standard nomenclature used in the VDI [3].

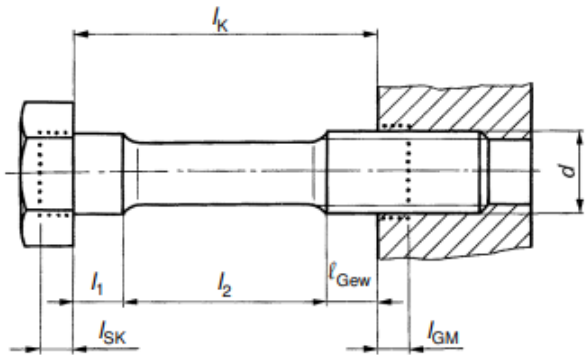

Figure 2: Bolt Sections VDI 2230 Part 1 5.1 [3]

The bolt resilience found using section 5.1 of the VDI 2230 describes the sections of a bolt according to figure 2. The bolts sections (i) each have individual areas (A_i) and lengths (l_i). Using the sections defined in figure 2 the resilience of the sections (δ_i) of the bolt can be numerically determined and used to find the resilience of the entire bolt (δ_s) using equation 1.

$$\delta_s = \delta_{sk} + \delta_i + \delta_{i+1} + \cdots + \delta_{Gew} + \delta_{GM} \quad (1)$$

Where each individual section's resilience is related to the geometry and modulus of the material (E_i) using equation 2.

$$\delta_i = \frac{l_i}{E_i * A_i} \quad (2)$$

The nut or the tapped hole region's resilience (δ_{GM}) is composed of both the resilience at the minor diameter of the bolt thread (δ_G) and the resilience in the nut or tapped hole (δ_M). According to the VDI these resiliencies are calculated with substitutional extension lengths. The VDI cites Schneider [7] and Watcher [8] for the study of the substitutional extension lengths. Lori and Watcher's work produced equations 3, 4, 5 and 6 where nominal bolt area (A_N) and minor area of the bolt (A_{d3}) are used to find each section resilience.

$$\delta_M = \frac{l_M}{E_s * A_N} \quad (3)$$

$$\delta_G = \frac{l_G}{E_s * A_{d_3}} \quad (4)$$

These resilience's are calculated using substitutional extension lengths (l_M) and (l_G). Note l_M is dependent on the joint type. Equation 5 and 6 are used to find the substitutional extension lengths for though bolted joints.

$$l_M = 0.4 * d \quad (5)$$

$$l_G = 0.5 * d \quad (6)$$

The resilience of the bolt head is found using equation 7 derived by Melino [9] for bolts with drilled out centers or strain gauge bolts along with equation 8 used to find the

substitutional extension length for (l_{SK}) for the hexagonal bolt head credited in the VDI to Lori [10].

$$\delta_{sk} = \frac{l_{SK}}{E_s * (A_N - 0.18A_{g)}} \quad (7)$$

$$l_{SK} = 0.5 * d \quad (8)$$

The resilience of the loaded, unengaged part of the thread (δ_{Gew}) is calculated using the area of the minor diameter of the bolt (A_{d3}). The extension length in this case is the length of the unengaged part of the thread that is loaded (l_{Gew}). Equation 9 is used to find $\delta_{Gew.}$

$$\delta_{Gew} = \frac{l_{Gew}}{E_s * A_{d_3}} \quad (9)$$

2.2 VDI 2230 5.1.2 Clamped Part Resilience

To calculate embedment the resilience of the clamp part must also be calculated. The resilience of the clamped part is calculated using section 5.1.2 of the VDI 2230. Figure 3 shows how the stress (σ_y) moves though the clamped part. As the distance from the bolt head or nut interface increases the axial compressive stress in the clamp part decreases. The zone under stress follows a parabolic curve. The VDI credits Lori [10], Fritsche [11], and Nguyen [12] for studying this phenomenon. To calculate the resilience

of the clamped part a substitutional deformation cone or simplified region is used following the line described by φ in figure 3.

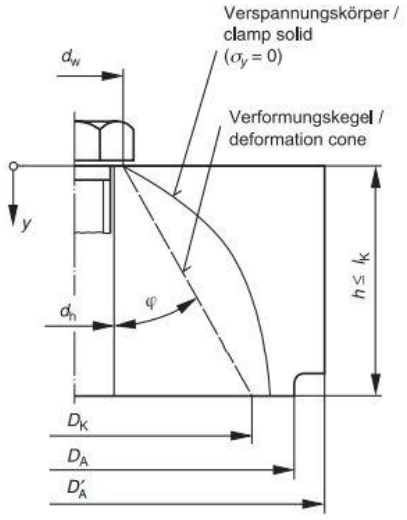

Figure 3: Clamped solid and calculation model [3]

The substitutional deformation bolted joint model is shown in figure 4. A deformation cone and sleeve are present in figure 4. If the deformation cone reaches the outer edge of the clamped surface a deformation sleeve must be included in calculations.

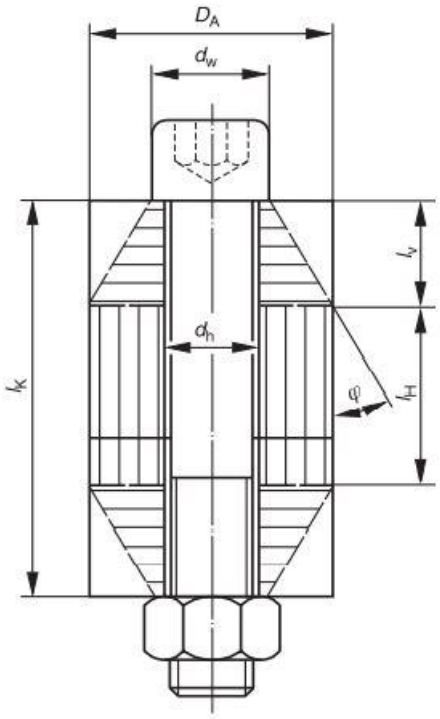

Figure 4: Simplified deformation cone [3]

A limiting diameter is used to define when a deformation sleeve needs to be accounted for in calculation. The limiting diameter is a function of the bolt bearing surface diameter (d_w), the clamp length of the bolted material (l_k), and the angle of the stress cone (φ). The limiting diameter ($D_{A,Gr}$) is calculated using equation 10.

$$D_{A,Gr} = d_w + w * l_k * \tan(\varphi) \quad (10)$$

The coefficient (w) for through bolted joints it is equal to 1. If the $D_A \geq D_{A,Gr}$ the model consists of only two stress cones, but if $D_A < D_{A,Gr}$ a deformation sleeve must be accounted for as well. For the case of $D_A \geq D_{A,Gr}$ equation 11 is used to find the clamped part's resilience, and if $D_A < D_{A,Gr}$ equation 12 is used in the calculation process. Equations 11 and 12 are accredited to Lori and Birger work [10][13].

$$\delta_p = 2 * \frac{\ln\left[\frac{(d_w + d_h) * (d_w + w * l_k * \tan(\varphi) - d_h)}{(d_w - d_h) * (d_w + w * l_k * \tan(\varphi) + d_h)}\right]}{w * E_p * \pi * d_h * \tan(\varphi)} \quad (11)$$

$$\delta_p = \frac{\left(\frac{2}{w * d_h * \tan(\varphi)}\right) \ln\left[\frac{(d_w + d_h)(D_A - d_h)}{(d_w - d_h)(D_A + d_h)}\right] + \frac{4}{D_A^2 - d_h^2}\left[l_k - \frac{D_A - d_w}{w * \tan(\varphi)}\right]}{E_p * \pi} \quad (12)$$

In finding the angle of the stress cone (φ) the VDI cites Lori, and Lange. [14][15]. It is defined as a function of the length to diameter ratio (β_L) and the diameter ratio (y), and is found using equations 13, 14, and 15.

$$\tan(\varphi) = 0.362 + 0.032 * \ln\left(\frac{\beta_L}{2}\right) + 0.153 * \ln(y) \quad (13)$$

$$\beta_L = l_k / d_w \quad (14)$$

$$y = D_A / d_w \quad (15)$$

For joints with clamped parts having differing Young's moduli such as when steel washers are used in an aluminum joint the deformation body need to be divided into not just a sleeve and cone, but also component deformation bodies having the same Young's moduli. For this calculation process the clamp length used in the resilience equations need to be further subdivided using equation 16. Therefore, the clamp length used is the sum of the associated m regions with the same moduli.

$$\sum l_i = l_K \quad (16)$$

Starting from the head or nut bearing surface the larger diameter of the preceding cone section applies as the bearing diameter (d_W) for the next deformation cone. This is outlined in equation 17.

$$d_{w,i} = d_w + 2 * \tan(\varphi) * \sum_{i=1}^{j} l_{i-1} \quad (17)$$

The resilience of the individual sections of different moduli can then be calculated using equations 11 and 12 shown above.

2.3 VDI 2230 5.4.2 Preload Changes

Section 5.4.2.1 of the VDI is the current state of the art regarding references for calculating embedment. Embedment is related to the loss of preload (F_z), the stiffness of the bolt (δ_s) and the stiffness of the clamped material (δ_P**)** using equation 18.

$$F_z = \frac{f_z}{(\varphi_{s+}\varphi_P)} \tag{18}$$

The VDI cites Ba-Saleem [2] who determined amount of embedding has been proven to depend on the working load, number of joint interfaces, and the roughness of the clamped material's interfaces that are in contact. Ba-Saleem's reference guild to embedment in steel bolt joint interfaces is shown in table 1. The VDI also states the amount of embedding in aluminum joints is expected to be greater than steel [16].

Table 1: Ba-Saleem's guild to embedment [2]

Average roughness height R_z according to DIN 4768	**Loading**	**Guide values for amounts of embedding** in µm		
		in the thread	per head or nut bearing area	per inner interface
< 10 µm	tension/compression	3	2,5	1,5
	shear	3	3	2
10 µm up to < 40 µm	tension/compression	3	3	2
	shear	3	4,5	2,5
40 µm up to < 160 µm	tension/compression	3	4	3
	shear	3	6,5	3,5

2.4 ISO 4287 Measuring Roughness

Quantifying the surface roughness of materials is covered in the ISO 4287 [17]. The roughness of material surfaces is measured using a profilometer. Modern laser profilometers read the geometry of the surfaces and calculate the arithmetical mean roughness (R_a) and mean roughness depth (R_z) values. An example surface profile is shown in figure 5.

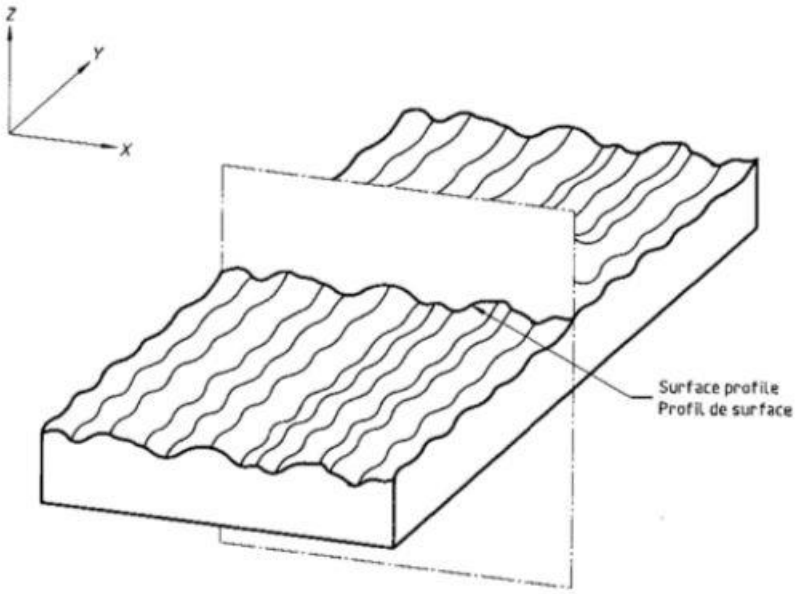

Figure 5: Surface profile measurement [17

Ra is determined using equation 19. Ra is visually represented in figure 6 [17].

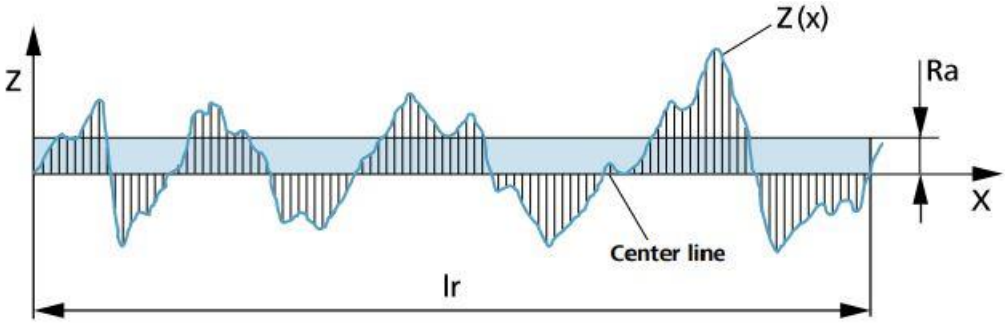

Figure 6: Ra visual representation [17]

Rz is determined using equation 20, and a visual representation of Rz is shown in figure 7.

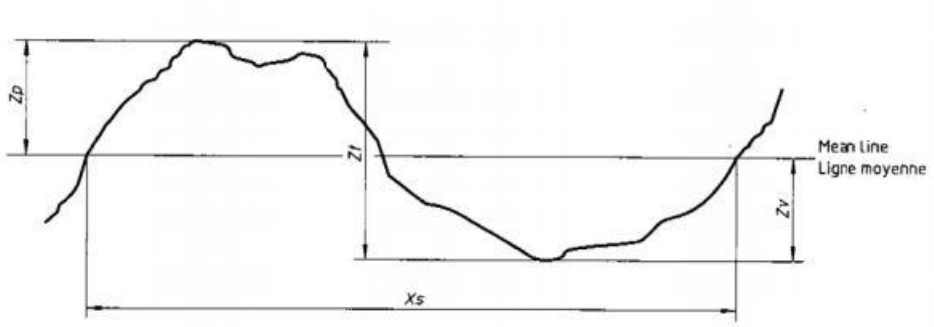

Figure 7: Rz or mean line visual representation [17]

$$R_a = \frac{1}{n}\sum_{i=1}^{n}|Z_i| \tag{19}$$

$$R_{z(ISO)} = \frac{1}{n}\left(\sum_{i=1}^{n} p_i - \sum_{i=1}^{n} v_i\right) \tag{20}$$

2.5 Muhamad Ba-Saleem – Relaxation Testing

Muhamad Ba-Saleem dissertation “Theoretische und experimentelle Untersuchungen der Setzverluste an Schraubenverbindungen” (“Theoretical and Experimental Investigations of the Setting Losses of Screw Connections”) is the primary source regarding embedment in the VDI [2]. He performed physical experiments on bolted joints utilizing ISO 4014 M10 and M8 bolts clamping C45 (AISI 1045) steel. Ba Saleem did not state the bolt material, or if the 1045 steel was hot or cold rolled. The joints in his experiments were loaded in shear, axially, and not loaded (static). The strain was monitored in the joint using strain gauges fitted to bolts both axially and radially. Ba-Saleem experimented with how bolt size (d), assembly force (F_M), clamp length (l_K), surface roughness ($R_{z\,(DIN)}$), and the number of contact interfaces (n_I) affected the

assembly preload losses though embedment. Ba-Saleem created table 1 used in the VDI 2230. Ba-Saleem used a stylus type linear profilometer to measure his specimen's surface roughness, and measured roughness with the stylus tip transverse to the machining direction. Ba-Saleem's testing showed that setting time in bolted joints lasts longer than 24 hours, and a settling time of 72 hours should be used for static testing. Ba-Saleem stated that dynamic testing was concluded after 10^6 cycles from the UTM but did not state the frequency at what the load fluctuated. He determined that embedment is directly related to surface roughness, number of contact interfaces, and assembly preload. Ba-Saleem also concluded that axial dynamic testing embedment amounts do not vary from static testing, and shear testing caused a higher loss in preload then both axial and static testing.

2.6 Masayuki Tendo & Nariam Afzali – Relaxation Testing

Afzali experimented with preload losses in stainless steel bolted joints [18]. Afzali used load cells in experiments with stainless steel bolts, and strain gauges for carbon steel experiments. Viscoelasticity was the stated reason for doing so. Viscoelasticity describes the rate-dependent inelastic behavior of solids, meaning that the deformation of the material depends on the rate at which the load is applied. This phenomenon occurs more in stainless steel then carbon steel because carbon steel bolts experience dynamic strain aging at room temperature. Afzali cited Tendo's work on this principal [6]. Tendo research yielded figure 8. Tendo noted that the carbon steel's creep rate could not be observed after several hours while the Type 304 steel's creep continued increasing after 1000 hours. Carbon steel also experience much less creep stain in comparison.

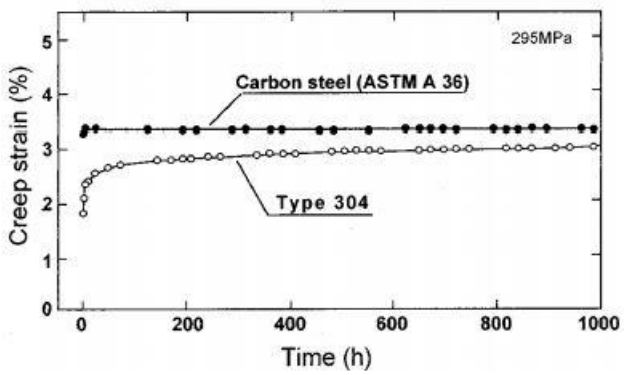

Figure 8: Creep Strain Carbon Steel and Type 304 Stainless [6]

Afzali monitored preload loss in bolted joints using EN ISO 4017 A4 austenitic stainless steel M16 Bumax 109, M16 Bumax 88, and M20 Bumax 88 bolts. The initial preload used for each test was 70% of the corresponding bolts tensile strength. The bolted material or plates used in this experimentation were carbon steel and austenitic, ferritic, duplex, and lean duplex stainless steel. Austentic, ferritic, duplex, and lean duplex are all categories of structural stainless steels distinguished by the microstructure and composition of the material. No surface treatment was done to the stainless-steel plates, but the carbon steel was shot blasted. The joints were not loaded externally, so Afzali's tests were performed over multiple days to allow the relaxation in the joints to stabilize. Afzali's experimentation yielded the results displayed in table 2.

Table 2: Afzali loss of preload testing results

Specimen ID	Number of Tests Performed	Bolt Material Class	Clamped Plates		Initial Preload (KN)	Loss of Preload	
			Material	Thickness [mm]		days	min/max (%)
M20 x75 mm							
CS	2	109	Carbon Steel	20	172	68	5.2/8.1
M20x100 mm							
SS01	12	Bumax 88	Austenitic	16	137	14	3.7/6.0
SS02	12		Ferritic			14	3.4/4.7
SS03	8		Duplex			55	3.9/5.0
SS04	3		Lean Duplex			14	4.0/4.5
M16 x 100 mm							
SS21	12	Bumax 88	Austenitic	8	88	14	3.9/5.5
SS22	12		Ferritic			14	3.5/5.0
SS23	12		Duplex			14	3.9/5.8
SS24	3		Lean Duplex			14	4.9/5.5
SS26	2	Bumax 109	Austenitic		110	14	5.7/6.6
SS27	2		Ferritic			14	4.2/4.9
SS28	12		Duplex			55	4.2/5.6

2.7 Xiao-Ping Pang – Material Modulus

Pang studied the physical properties of high strength bolted materials at elevated temperatures. He performed tensile tests on carbon steel with property classes 8.8, 10.9, and 12.9. Pang used threaded coupons machined out of each property class. The bolts used and a coupon are shown in figure 9. The coupons were threaded to prevent the samples from slipping in the testing machine's jaws. Pang utilized a servo-controlled loading system (Instron 8862), and a high-temperature extensometer with a gauge length of 12.5 mm in testing.

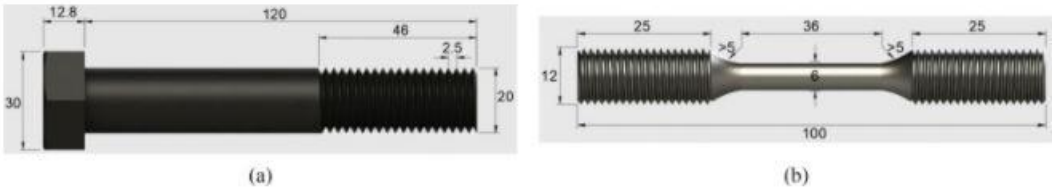

Figure 9: Bolt (a) and Coupon (b) dimensions [19]

At 20° C or approximately room temperature, they found elastic modulus of the 8.8, 10.9, and 12.9 bolts were 211.7, 214.5, and 211.1 GPa, respectively. Pang's values for material modulus were compared to values found in this experiment.

2.8 Paul Melino

Paul Melino [9] developed the embedment testing methodology used in the control testing and some of the dynamic testing for this paper. Melino utilized M10 carbon steel bolts in relaxation testing on clamped cold rolled 1045 steel and attempted to draw a correlation between the number of inner interfaces in bolted joints and embedment. His experiments were performed with no external loading over the course of three days. Melino experimented with bolted joints having one, two, three, and four clamped parts. The results from this testing are shown in figure 10. The results from his testing with one clamped part is used as a reference for testing done in this experiment. Melino concluded that as the number of contact interfaces increased the amount of embedment generally increased as well.

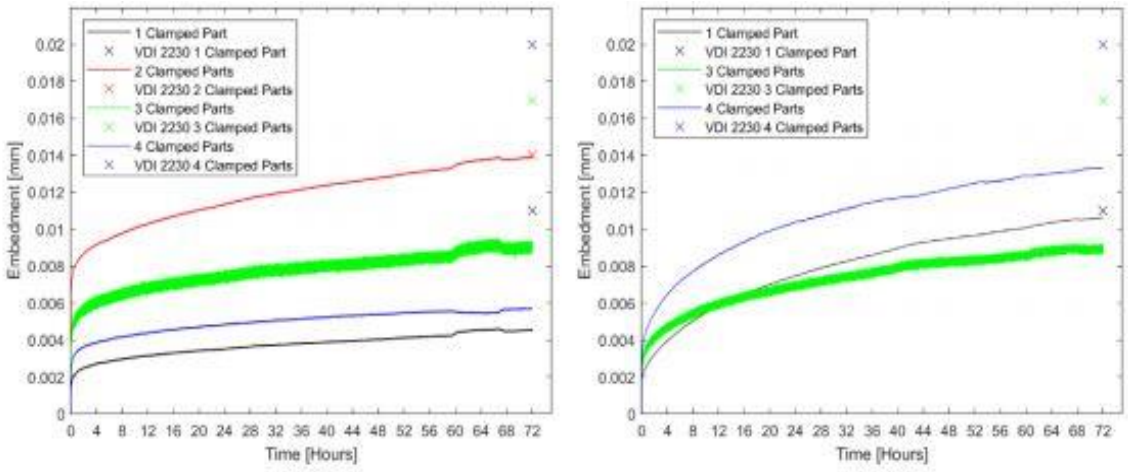

Figure 10: Melino embedment testing [9]

2.9 C.L.J. Den Otter

Otter performed relaxation and creep testing [20]. Otter used 5454O and 5083 0/H111 aluminum alloys during his creep testing. The surfaces of the aluminum were both grit blasted and tested as delivered. His creep tests were performed for less than one day. The results from Otter's creep testing are displayed in figure 11.

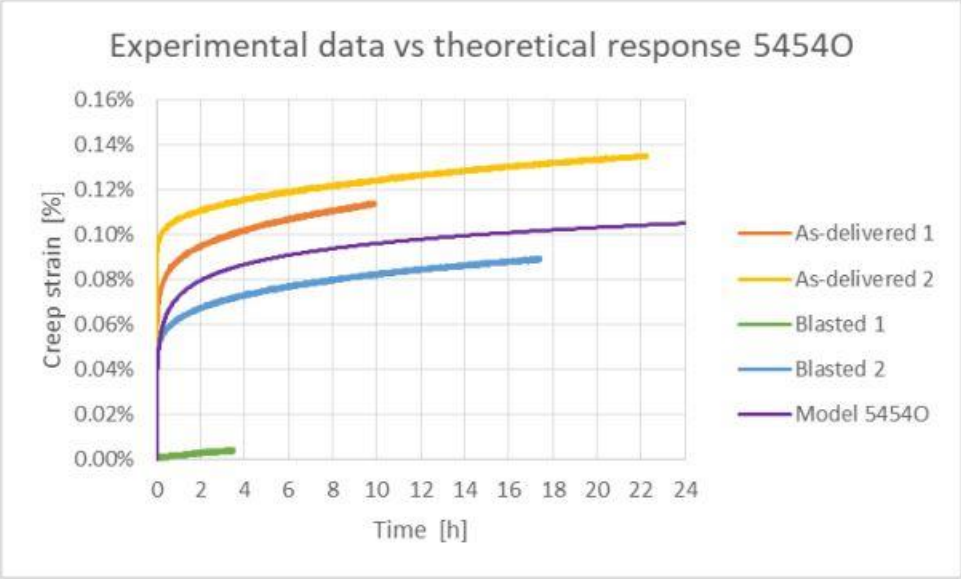

Figure 11: Otter aluminum creep testing [20]

Otter concluded that the grit blasted surfaces are less susceptible to losses due to creep stain because grit blasting causes a hardening effect in the material. It was also noted that most of the creep occurred within the first 2 hours of Otter's testing. Otter estimated the amount of embedment that occurred in the interface to be approximately 7.75 µm. Otter also concluded that at a given stress alloys with higher proof stresses are less susceptible to creep/embedment. He also noted that stainless steel exhibits increasing stress relaxation with increasing preload forces and stated that bolted joints that combine materials having varied thermal expansion coefficients are more susceptible to preload changes caused by changes in temperature.

3.0 METHODOLOGY

3.1 Bolt Manufacturing and Calibration

The bolt calibration techniques used in this research are the same as the methods used by Melino [5]. The strain gauge bolts were fabricated from property class 8.8 and 12.9 DIN-931 M10 x 1.5 x 60 mm bolts. Tokyo Measuring Instruments Laboratory Co., Ltd BTMC-1-D16-003L quarter bridge strain gauges [21] were inserted into 1.6 mm holes drilled 20.23 mm down though the center of the bolt head. The strain gauges, the drilled-out bolt head and finished strain gauge bolt are pictured in figure 12.

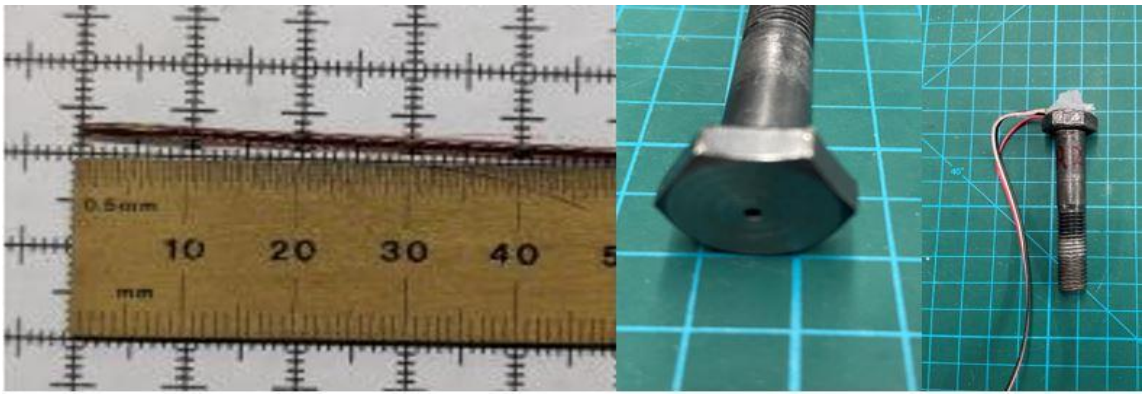

Figure 12: Strain gauge, Bolt Hole, and finished strain gauge bolt

The strain gauges are fitted to the bolt using a cyanoacrylate adhesive. This adhesive bonds the strain gauge to the wall of the bolt shank. The stain gauge leads were soldered to terminals glued to the bolt head and wired to a RJ50 10P10C slim breakout board by Winford. The top surface of the bolt was covered in silicone to prevent damage to the gauge leads.

Once bolts are ready to be calibrated, they are loaded in the UTM with collars for the machine's jaws to grip. Figure 13 displays the finished strain gauge bolts loaded into the UTM for calibration.

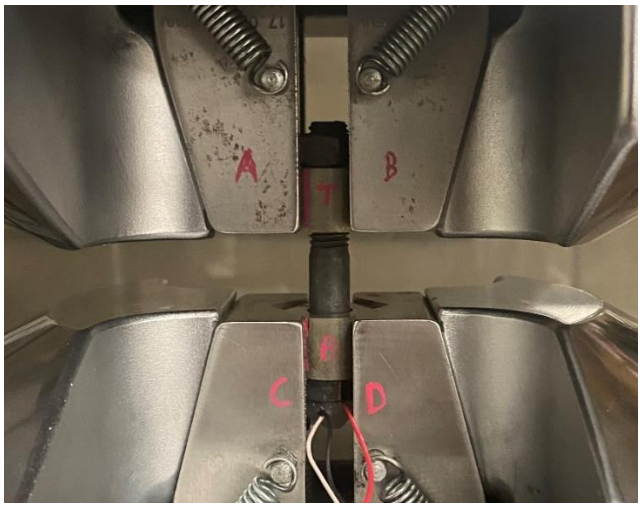

Figure 13: Bolt calibration setup

This procedure utilized an MTS 370 Landmark UTM with a +/-100 KN capacity. The bolted joints were loaded by the UTM while the applied force, displacement, strain from the gauge, and ambient room temperature was recorded. The force per unit strain coefficient of the strain gauge bolts could then be determined by finding the linear best fit of the strain vs applied force. The experimental resilience of the bolts could also be determined using this procedure by using displacement from the fixture and the resilience of the fixture in the UTM. In this experiment, the resilience of the fixture used was unknown, so the resilience calculations laid out in the VDI were used to find bolt resilience.

3.2 Bolt Modulus Testing

The class 8.8 and 12.9 DIN-931 bolts were machined into cylinders with a lathe so they could be inserted into a UTM for modulus testing. Figure 14 shows the bolts after the machining process.

Figure 14: Class 12.9 (left) and 8.8 (right) cylinders

The cylinders were inserted into the UTM and pulled until the material's modulus could be extracted from the data collected. The displacement of the cylinders was measured with an extensometer equipped to the cylinders shank. The grooves on the cylinder ends allowed the UTM to better grip the specimens much like Pang's testing [19].

3.3 Specimen Manufacturing

The current VDI standards for embedment relate embedment to material roughness. Specimen tested in this experiment were maufactured to have specific three specific roughnesses. Specimens were maufactured to have target roughnesses (Rz) of 130, 30, and < 15 µm to compare to the current standard. This was done by using a fly cutter pictured in figure 16. The fly cutter was used in inconjuntion with a CNC mill. The mill was programed through trial and error to give the correct roughnesses to the samples each time. Spindle speed, feed rate, and cut depth were the vaiables manipulated to give the correct roughness for both the 130 and 30 µm. The machining parameter found for both Rz 130 and 30 µm was a spindle speed of 52.4 rad/sec, feed rates of 560 and 152

mm/min, and cut depths of 0.18 and 0.054 mm respectivly. The < 15 µm samples were cut, faced with a mill, and polished using 600 grit sandpaper to achive the small roughness. A picture of the 130 µm pucks is shown below in figure 15.

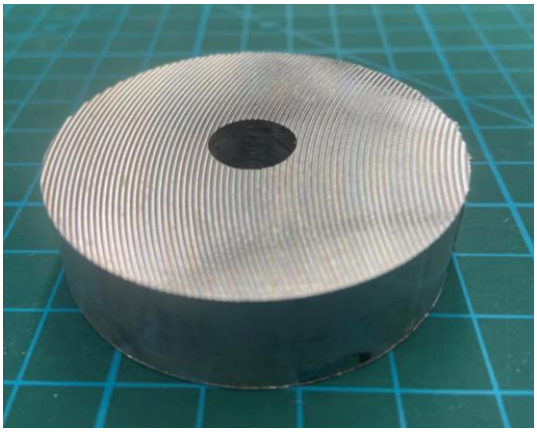

Figure 15:Rz 130 um roughness samples

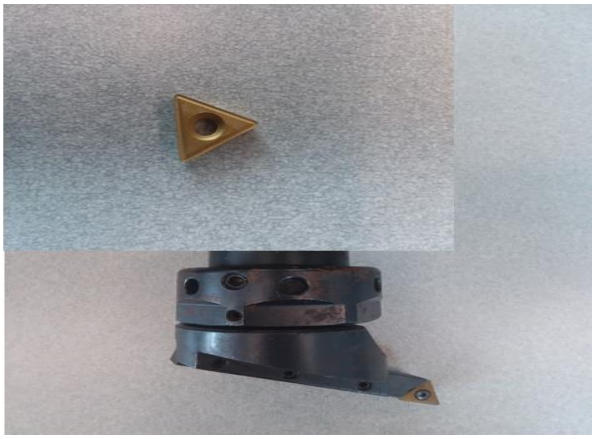

Figure 16: Fly cutter and carbide insert

The bit used in the fly cutter was an Interstate TT322 TCN55 carbide insert (ISO 160312) 19 degrees from the surface of the part. The insert is pictured also in figure 16. After the pucks were machined a Keyence laser microscope was used to measure the roughness of the pucks. The roughness was measured according to the ISO 4287 standard, and each sample was measured multiple times [16][17]. After confirming the CNC mill's ability to produce consistent roughness values it was deemed unnecessary to measure roughness for each sample. An example of a report from the microscope and the microscope itself are pictured below in figure 17.

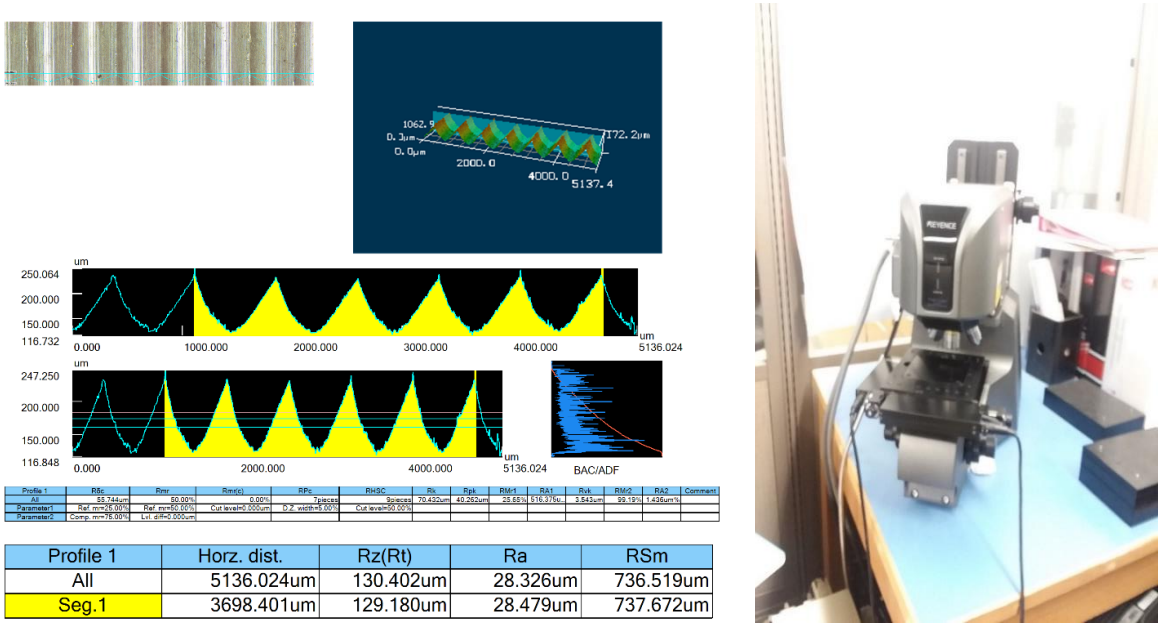

Profile 1	Horz. dist.	Rz(Rt)	Ra	RSm
All	5136.024um	130.402um	28.326um	736.519um
Seg.1	3698.401um	129.180um	28.479um	737.672um

Figure 17: Roughness Report, Keyence Laser Microscope

3.4 Friction Coefficient Testing

To understand what shear force could be applied to the joints friction coefficient testing was carried out. Friction coefficient tests were performed on both the 6061-T6511 aluminum and the cold rolled 1045 steel with surfaces machined to roughness of 130, 30, and <15 um. These tests were used to determine the force that could be applied to the joints in shear without causing the joint to slip. The tests were performed with a constant displacement setup moving at 5 mm/min. The MTS Insight 5 used took force and displacement readings at 20 Hz. The samples were loaded with a 54.5 N weight placed on top of the sample. Figure 18 displays pictures of the slip testing setup.

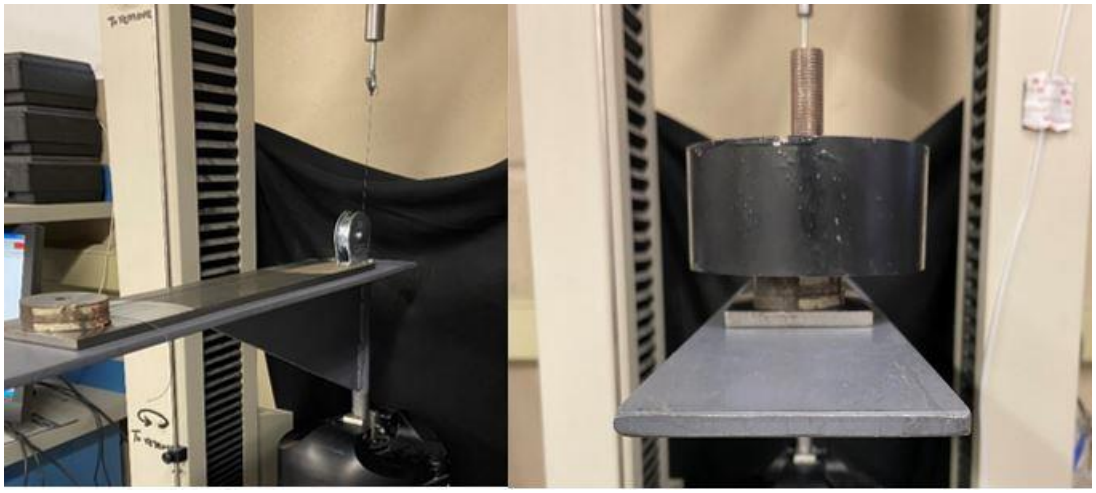

Figure 18: Slip testing fixture

3.5 Torquing Test Specimens

The samples in this experiment were tightened using an AIMCO electric torque wrench pictured below in figure 19.

Figure 19: AIMCO electric slip clutch torque wrench

A precision slip clutch was used so, that the specimens would be clamped in a consistent, and quick manner much like the bolting of joints on a production line in a factory. The wrench rotates at 170 RPM and its torque was set to target approximately 66% of the max preload of the class 12.9 M10 bolts used is this experiment. Given that the min preload for yield for the class 12.9 M10 bolts is 63.8 KN the target preload was 42.2 KN. Because the slip clutch doesn't have a torque display or setting, the correct tightening torque was found though trial and error using the strain readings from the strain gauge bolts. The force per unit strain coefficient of the bolt was used to find the

target strain. Tightening using the torque method is one of the most unreliable as far as achieving precise tightening during each test, so the threads on the bolt were lubricated with LB 8060 Loctite anti seize to limit the influence of frictional scatter while tightening.

3.6 Dynamic Testing Procedure

Before loading in the shear fixture specimens were tightened down inside of a 90-degree crows foot clamped inside of a vise grip. The tightening station is shown in figure 20. The custom shear fixture used in experimentation is shown in figure 21.

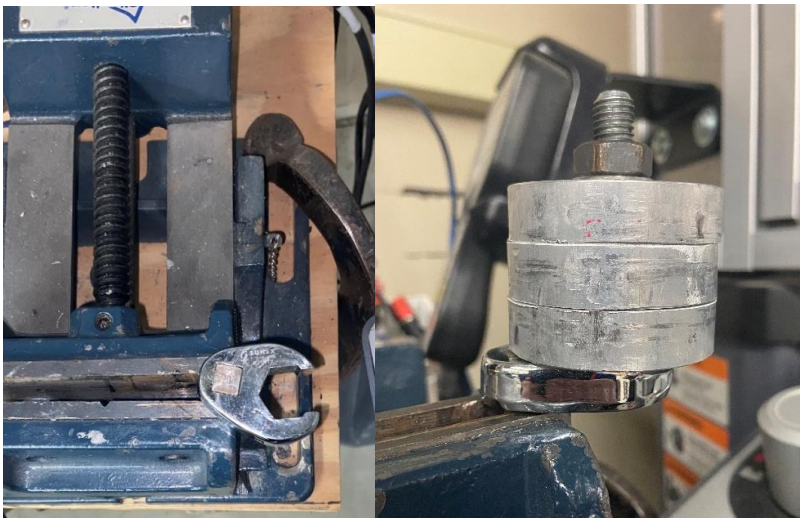

Figure 20: Joint tightening station

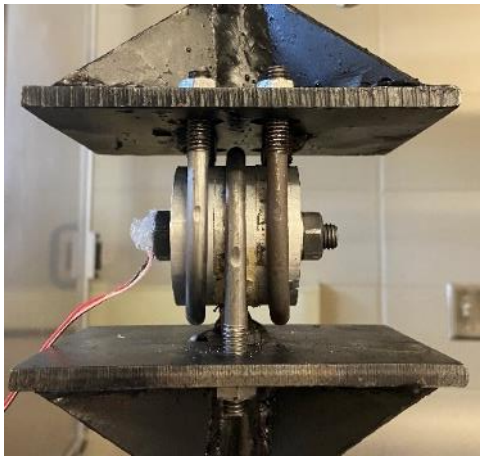

Figure 21: UTM shear fixture

The forces applied by the fixture are not directly in line with the interfaces of the bolted joint. As a result, there is a bending load that caused an uneven loading in samples. This is shown in a free body diagram in figure 22. The bolted joints are rotated 90 degrees once during every test because of this phenomenon. This ensures that the force being distributed on the samples is uneven, all quadrants of the samples experience the same loading.

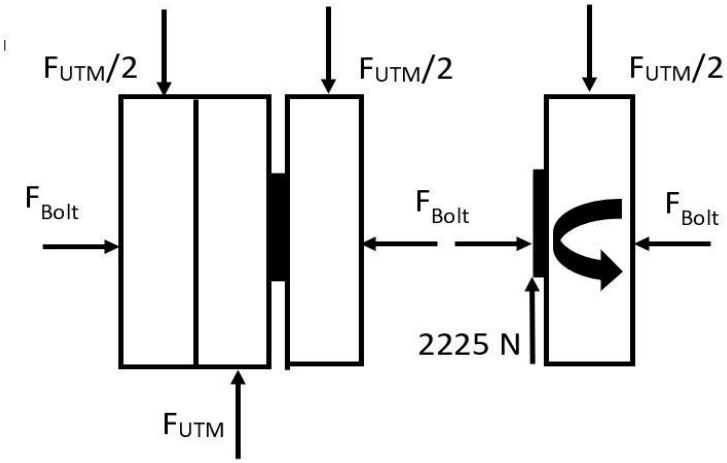

Figure 22: Free body diagram shear fixture

Tests were performed with three different shear forces for each roughness. The UTM applied loads for each roughness were 14457 N, 6672 N, and 3336 N. The steel tests were able to be conducted without washers because of CR 1045 steel's high surface pressure at yield while 6061-T6511 aluminum's bearing yield strength (386 MPa) is much lower. See appendix section 6.1 for the material properties table from the VDI. Washers increase the bearing surface diameter to lower the surface pressure on the material. The washers used in this experiment were DIN 125 bumax 109 stainless steel. Figure 23 displays models of the cross sections of the aluminum joint with washers and steel joints without washers. The bearing stress was calculated and recorded for each test.

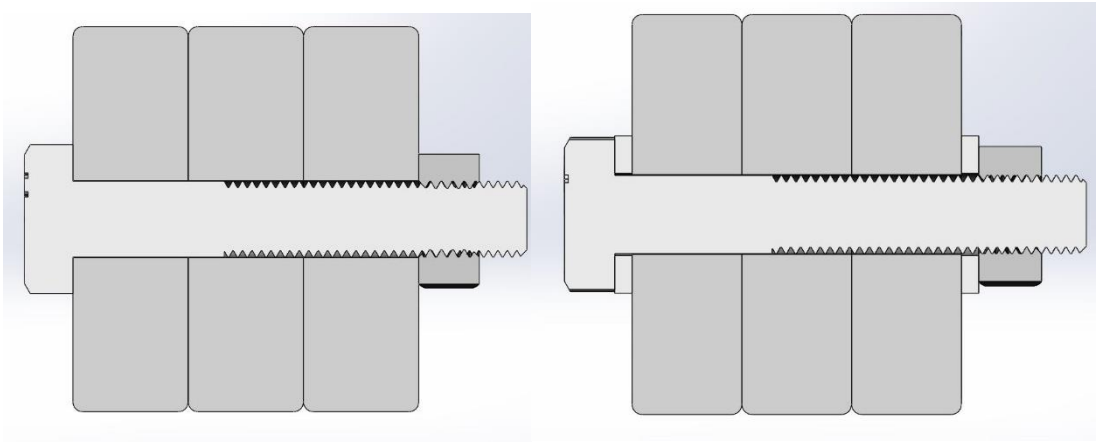

Figure 23: a) Steel Bolted Joint b) Aluminum Bolted Joint

3.7 Dynamic Testing Data Monitoring

The test setup is powered by a laptop running LabVIEW in conjunction with National Instrument's NI cDAQ-9172 which records the strain, the MTS machine's applied force, time, and the temperature of the room. The strain, temperature and the MTS machine's applied force are read through National Instruments NI 9237, NI 9213 and the NI 9206 modules respectively. The NI 9213 utilizes a T-type thermocouple to read the temperature of the room, and the NI 9206 is setup to read a voltage output from the UTM corresponding with the force the machine is currently applying. The program took readings at 1.4 Hz. Temperature does affect the readings on the strain gauges, and because of this a reference gauge was introduced to limit the error resulting from changes in temperature. A quarter bridge type 2 was used to setup a reference or dummy gauge. A wiring schematic for the quarter bridge 2 is shown below in figure 24. This was implemented with a RJ50 10P10C Slim Breakout Board by Winford that was used to connect the strain gauges to the NI 9237 DAQ module. This compensation does not account for the clamped material's changes in deformation due to temperature changes, however. Temperature change from the tightening temperature was recorded for each test

but was not accounted for in calculations. Tests with large outliers in temperature differences were discarded. Static tests that had to be tested much longer than dynamic tests were kept in a waterproof container inside of a water bath set to slightly above the room temperature (32°C) to limit the influence of temperature.

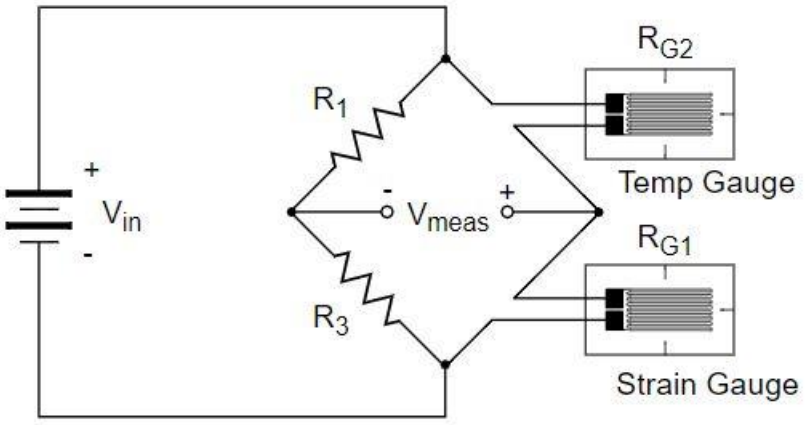

Figure 24: Quarter bridge type 2 (Website)

3.8 Embedment and Clamp Length

One of the conclusions from Ba-Saleem's research [3] was that embedment remains constant regardless of clamp length, but Ba-Saleem only experiment with 1045 steel. It is unknown if this phenomenon holds true for bolted joints of aluminum. To test the effects of clamp length on the amount of embedment in aluminum bolted joints relaxation tests were performed at three different clamp lengths within the M10x1.5x60 mm bolt's clamp range. Clamp lengths of 50, 42, and 34 mm were tested. Property class 8.8 bolts were used in this portion of the experiment. This was the only testing done that utilized class 8.8 bolts. The same testing procedure outlined in section 3.5 and 3.6 of this report was used in this testing. The joints were loaded to 75% of the proof load of the bolt, and externally loaded by the fixture at 4450 N.

3.9 Control Testing

To differentiate the embedment between contact interfaces, and the embedment that occurs in the bolt, nut, and thread interfaces control testing needed to be performed with joints where the inner contact interfaces were no longer present. Control tests were performed with one solid specimen instead of three separate specimens. The embedment that occurs in this system can then be compared to testing with joint interfaces having varying roughness to find the added embedment of each test based on the surface roughness of the material. These tests because the specimens are one solid piece were not externally loaded in the same way as tests with inner contact interfaces. Instead of externally loading the control tests the test were performed without loading over multiple days. The static testing values according to Ba Saleem were approximately the same as dynamic or externally loaded tests. [3] The longer the tests are performed the more temperature changes can affect the system. The static test specimens were placed in a waterproof zip lock bag inside of a temperature-controlled water bath set to above room temperature. The bolted joint components are placed in the bath before tightening and removed temporarily for tightening. The joints were tightened as fast as possible to avoid excessive cooling of the specimen. The usual time to tighten average around 20 seconds. The joints were then moved back into the bath. The control tests were ended after 3 days, Ba Saleem reported that after 3 days embedment slowed to a negligible amount. The testing procedure outlined by Melino was the procedure used in this portion of the experiment. [9] The strain was monitored using the same apparatus as described in section 3.7 but was not monitored continuously. For the testing in this paper, only the beginning and end of the tests were monitored due to a lack of DAQ availability.

4.0 RESULTS

4.1 Bolt Calibration

A typical force vs strain plot is shown in figure 25 with the force per unit strain coefficient and R^2 value displayed.

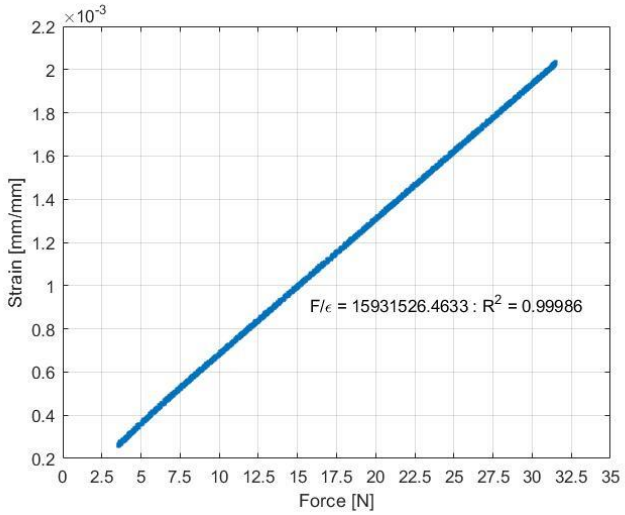

Figure 25: L1 Strain vs Force

Table 3 displays data collected during calibration for each 12.9 bolt used in this experiment.

Table 3: Class 12.9 strain gauge calibration data

Bolt Index	R1	R2	R3	L1	L2
Force/Strain [N/mm/mm]	16025276	16253763	16355638	15931526	16046449
R^2	0.9998	0.9998	0.9979	0.9998	0.9998
E [GPa]	215	219	220	214	216

The approximate modulus was found by dividing the force per unit strain coefficient by the bolt's area accounting for the loss of material in the bolt head. The average modulus found using this method was 217 GPa. This is comparable to Pang's testing [19] but was 2.75% greater than Pang's experimental modulus for class 12.9 steel (211.1 GPa). The data collected during the ISO class 8.8 bolt testing is presented in table 4.

Table 4: Class 8.8 strain gauge calibration data

Bolt Index		A1	A2	A3	A4
Force/Strain	[N/mm/mm]	15211470	15161475	15219648	15337680
R^2	NA	0.9984	0.9998	0.9998	0.9997
E	[Gpa]	205	204	205	207

The average modulus found from the force per unit strain coefficient for the ISO class 8.8 bolts calibrated in this experiment was 205 GPa. Pang's experiment modulus for ISO class 8.8 bolts was 211.7, which was 3.21% different from the value found in this experiment.

4.2 Modulus Testing

Figure 26 and 27 show the plots of force vs extensometer displacement for the cylinders made of the ISO class 8.8 and 12.9 bolt materials.

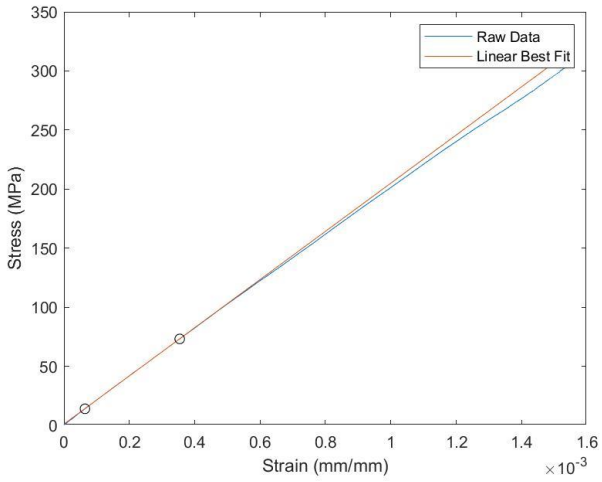

Figure 26: Class 8.8-cylinder test

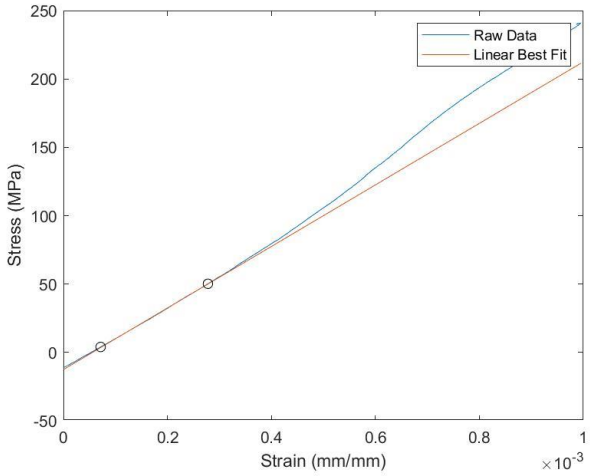

Figure 27: Class 12.9-cylinder test

The modulus found in the ISO class 8.8 testing was 204 GPa while the class 12.9 bolt's modulus was 225 GPa. This testing was used as a reference, but these modulus values were not used in calculation due to the low samples size of only one test per bolt material.

4.3 Friction Coefficient Testing

Each interface type was tested 7 times. The average slip coefficients for each roughness are pictured in table 5. The raw results are tabulated in the appendix section 6.2. For both the 6061-T6511 aluminum and the CR 1045 steel generally as the roughness of the samples increased the slip coefficients increased as well. Figure 28 display the slip coefficients for both aluminum and steel plotted vs the material roughness.

Table 5: Slip coefficient testing data

Roughness (Rz)(um)	<15	30	130
Al Slip Coef	0.20	0.22	0.33
FE Slip Coef	0.17	0.19	0.40

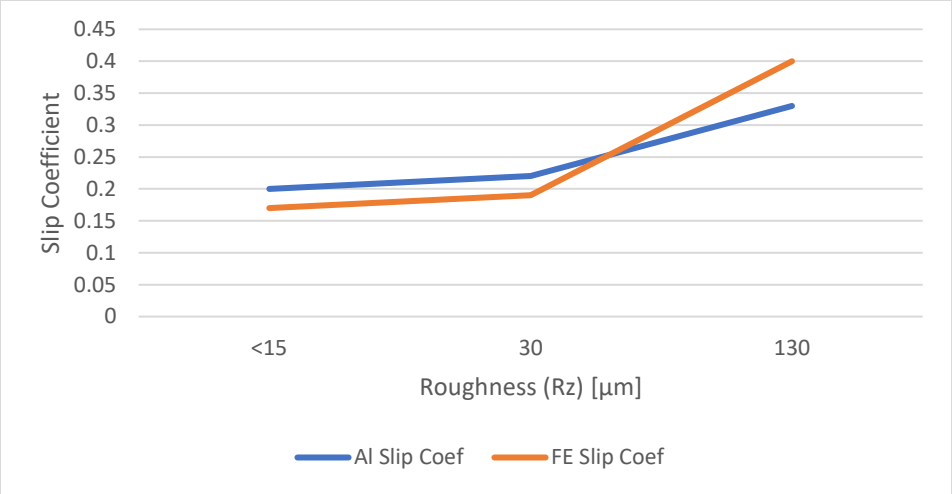

Figure 28: Slip coefficient and material roughness

4.4 Dynamic Testing

4.4.1 Testing Overview

During testing both time dependent and non-time dependent preload losses were observed. Figure 29 displays the strain gauge data collected during an aluminum Rz 130 µm test under an external load of 14457 N with the embedment plotted vs time. Figure 30 displays this data with the external applied force also plotted. The applied force appears to be solid but is fluctuating in a sine wave pattern.

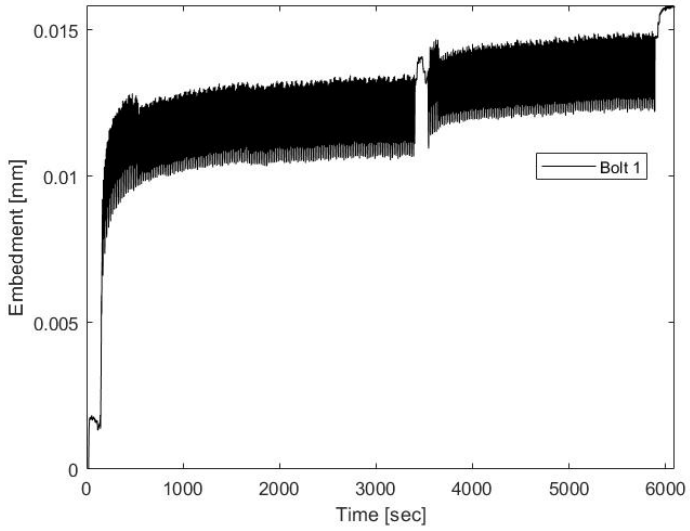

Figure 29: Aluminum embedment and time during loaded test

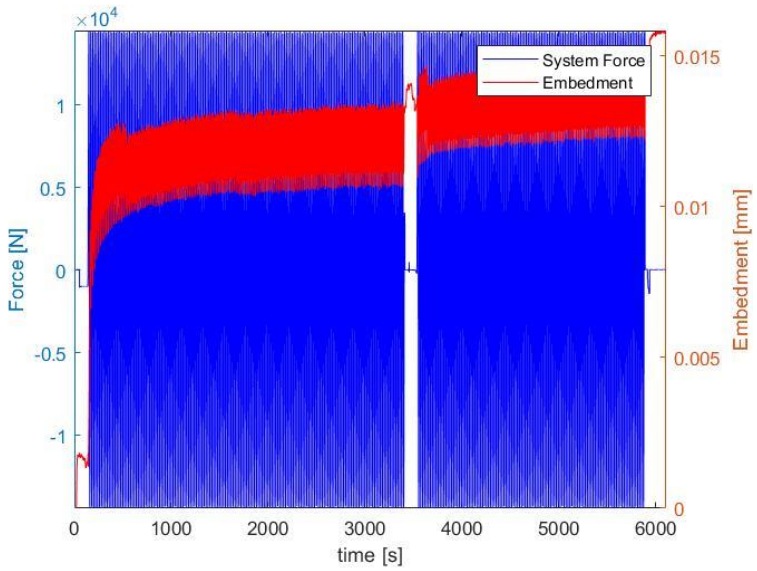

Figure 30: Aluminum embedment, applied force and time.

Most of the embedment that occurs in the system occurs at the beginning of the test as soon as the joint is loaded. Once the areas under contact in the inner interfaces of the joint plastically deform the surface area of the contact increased stabilizing the system under the given load. After the initial loading embedment still occurs but at a much slower rate. This is most likely due to the time dependent properties of aluminum. After the initial loading it appeared that the time dependent properties of the material were the major factor in determining preload losses. To see if the loading was affecting the time dependent properties of the material figure 31 was created.

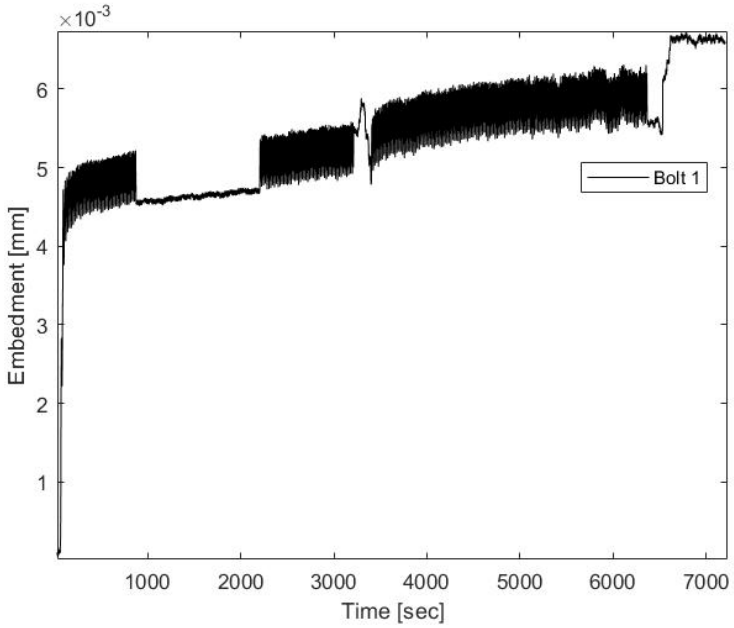

Figure 31: Steel embedment and time during loaded test

During the test in Figure 31 after the initial loading the loading was stopped between 1000 and 2000 seconds to see how the preload losses were affected. The rate of preload losses appears to be relatively unaffected by the lack of loading. Therefore, after the initial loading of the joints the property that most effects the preload losses are the time dependent properties of the material or the creep loss. It should also be noted that after the rotation of the sample at approximately 3000 seconds the loading increased the rate of preload losses, but again after the initial loading after rotation the preload losses became time dependent. This property held true for both the aluminum and steel tested.

4.4.1 Clamp Length Testing

Table 6 displays the average testing results for embedment vs clamp length testing. The raw results are tabulated in section 6.3 of the appendix. As the clamp length of the clamped material decreased the percent clamp load or preload loss increased while the amount of embedment remained approximately the same.

Table 6: Clamp Length Testing

Clamp Length [mm]	Max Pre-Load [N]	Preload Loss [%]	Embedment [µm]
50	24848	2.31	3.47
42	23655	2.91	3.46
34	24671	3.10	3.28

Using the average embedment found in testing (3.40 µm) the theoretical preload loss for varying clamp length was calculated and plotted vs the actual preload loss observed in testing in figure 32. The preload loss values found in this experiment at each clamp length was consistent with the expected loss using the found value for embedment.

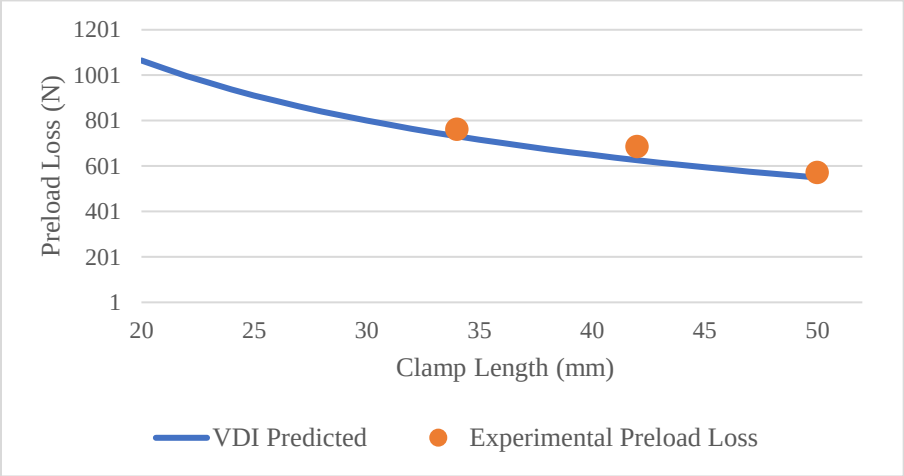

Figure 32: Preload Loss vs Clamp Length Testing

4.4.2 Roughness Testing Averages

Tables 7 through 9 display the average testing results for both aluminum and steel at each roughness and applied force from the UTM. For some tests, the UTM applied a load that was greater than the slip force of the joint. The lower roughness values were affected more by this phenomenon as they exhibited a lower slip coefficient. The testing with UTM applied loads of 14457 N in tables 7 and 8 were not completed because joints underwent complete and consecutive slip. Completed tests above the theoretical slip force rarely experienced joint slippage, but one or two non-consecutive slips was considered

acceptable during the length of the test. The groves at the interfaces most likely increased the surface slip coefficient as they embedded into each other during tightening. The raw data used to created tables 7 through 9 is tabulated in section 6.4 of the appendix.

Table 7: Average <Rz15 µm testing results

Clamped Material	Number of Tests	UTM Force [N]	Clamp Length [mm]	Initial Clamp Load [N]	Clamp Load Loss [%]	Embedment [um]
Aluminum	6	6672	46.5	43215	1.33	3.52
	5	11121	46.5	44938	2.16	7.17
	0	14457	NA	NA	NA	NA
Steel	6	6672	49.5	41670	0.74	1.58
	6	11121	49.5	41232	0.82	1.74
	0	14457	NA	NA	NA	NA

Table 8: Average Rz30 µm testing results

Clamped Material	Number of Tests	UTM Force [N]	Clamp Length [mm]	Initial Clamp Load [N]	Clamp Load Loss [%]	Embedment [um]
Aluminum	5	6672	44.7	41644	2.20	5.50
	5	11121	43.2	43779	2.85	6.89
	5	14457	44.5	44438	3.51	8.67
Steel	4	6672	49.5	42383	0.92	2.00
	5	11121	50	40399	1.72	3.57
	0	14457	NA	NA	NA	NA

Table 9: Average Rz130 µm testing results

Clamped Material	Number of Tests	UTM Force [N]	Clamp Length [mm]	Initial Clamp Load [N]	Clamp Load Loss [%]	Embedment [um]
Aluminum	6	6672	44.5	41120	2.64	6.31
	6	11121	45.5	43172	4.37	10.79
	4	14457	45	44170	7.69	19.28
Steel	5	6672	49.8	45499	1.91	4.66
	6	11121	49.3	42502	2.95	7.11
	6	14457	50	44119	3.90	9.38

Tests were conducted until strain changes moved to negligible levels or stopped after two hours of loading. The laboratory was not temperature controlled, but the two-hour time limit minimized the effects of temperature changes as it was found that the laboratory's ambient temperature changes remained within an acceptable range for

approximately two hours at a time. Opening of the laboratory's door and the initialization of the HVAC unit often caused test failure in the case of testing clamped aluminum, but clamped steel testing was much less susceptible to changes in temperature as the bolt and the 1045 steel have more similar coefficients of thermal expansion. The same procedure and limitations were still followed for steel testing to achieve testing consistency. The average temperature change for all testing was less than one degree Celsius. Samples were reused only three times in testing as retightening has been proven to decrease the effects of embedment by previous researchers [22], but testing conducted in this experiment showed little change with retightening. The low roughness, Rz <15 µm, samples were polished after every test as it was observed that consecutive clamping of the low roughness samples without repolishing increased preload losses.

4.4.3 Material Roughness and embedment

Figures 33 and 34 show plots of the experimental embedment plotted vs the specimen roughness at each force applied by the UTM. Figure 34 includes the expected embedment for bolted joints each roughness found in the VDI 2230 according to Ba Saleem. [3]

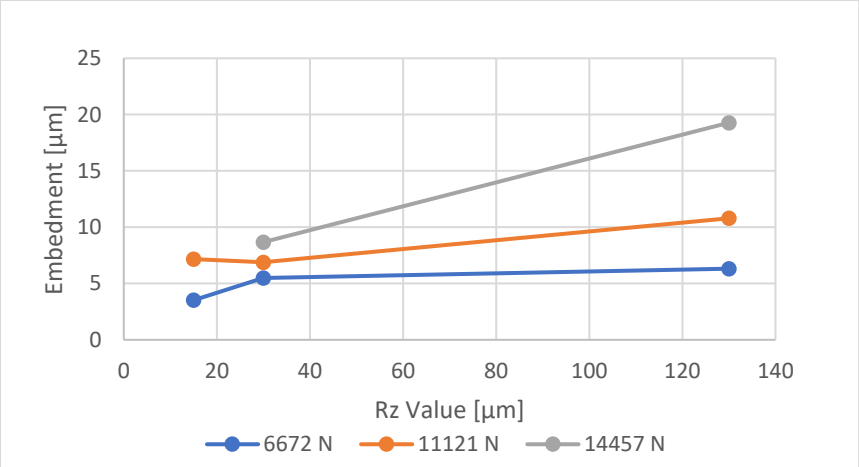

Figure 33: Aluminum embedment vs Roughness Value

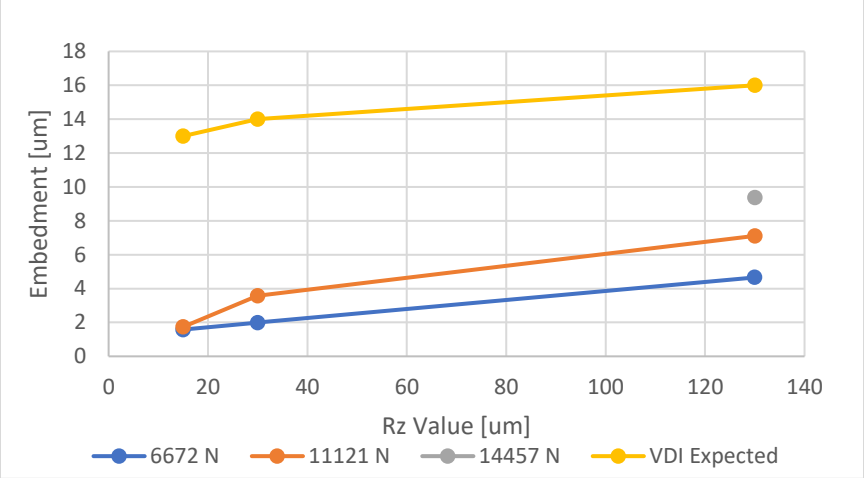

Figure 34: Steel embedment vs Roughness Value

Generally, as the roughness of the samples increased the amount of embedment that occurred increased as well.

4.4.4 Applied Force and Embedment

Figures 32 and 33 show the experiment embedment plotted vs the applied force by the UTM. The slip forces for each roughness value are also plotted.

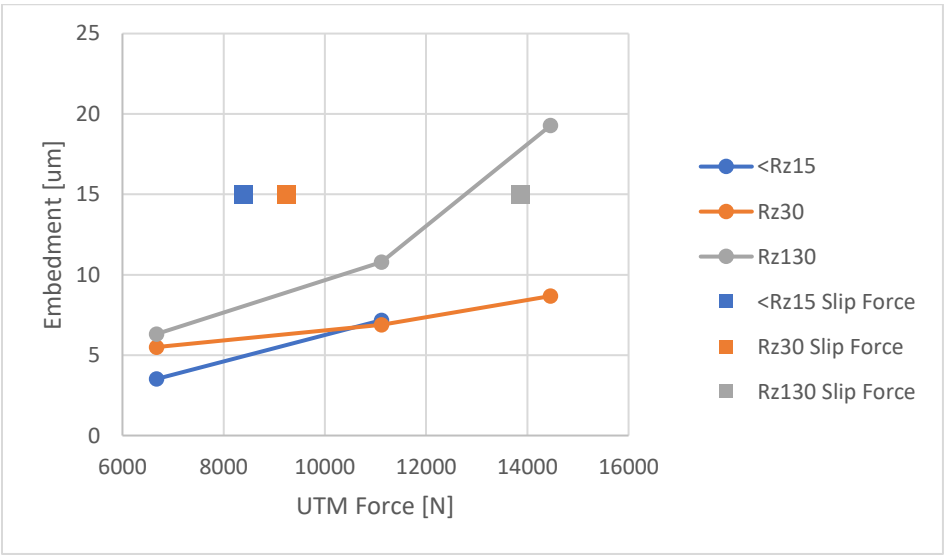

Figure 35: Embedment vs UTM force aluminum

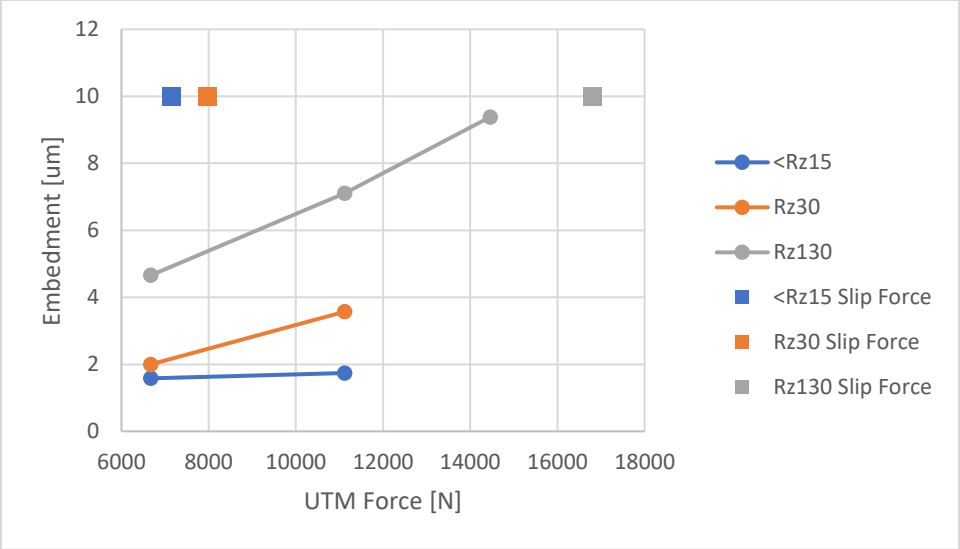

Figure 36: Embedment vs UTM force Steel

As the applied load from the UTM increased the embedment did as well. The rougher the sample the more the embedment increased with increasing applied force from the UTM.

4.5 Control Embedment Testing Results

The control testing done in this experiment were designed to measure only the time dependent properties of the bolted materials. The control testing done on the 1045 steel was unconclusive. The loss in strain during testing was approximately zero during the three-day period. A longer test should have been carried for the steel. Extrapolation from the existing data yielded results with obvious inaccuracy. The aluminum testing results are displayed in table 10.

Table 10: Aluminum control testing results

Material	Clamp Length [mm]	Max Preload [kN]	Preload Loss (%)	Embedment [µm]
Al	43.18	36931	2.30	4.87
	43.18	42712	1.90	4.64
	43.18	45007	2.79	6.25
	43.18	40912	4.70	8.02
Average	**NA**	**41390.17**	**2.92**	**5.95**

The average amount of embedment that occurred in aluminum control testing was greater than the externally loaded samples of the lowest roughness. The time dependent properties of aluminum allowed preload loss to continue for the entire duration of tests resulting in more preload losses due to creep. Therefore, Ba Saleem's conclusion that joints loaded dynamically in shear will have more embedment losses as statically loaded joints could be called into question for materials with higher rates of creep. No differing conclusion could be made in regard to the 1045 steel with the experimental data collected as the control tests experienced less embedment than the dynamic testing, but the dynamic testing also had more interfaces, which increase embedment losses.

5.0 CONCLUSIONS

The average force per unit strain coefficients found during calibration for both the ISO class 8.8 and 12.9 bolts were 15.2 and 16.1 MPa/(mm/mm) respectively. Therefore, the experimental modulus of the 8.8 and 12.9 bolts was approximately 217 and 205 GPa. The bolt material cylinder testing yielded modulus values of 204 and 225 GPa for the 8.8 and 12.9 bolts, respectively. The modulus values found during calibration were used in the embedment calculations in this experiment. They were both within approximately 4% of Pangs values.

As the roughness of both the aluminum and the steel increased the friction coefficient increased as well. The Rz130 μm samples had much higher slip coefficients than the lower roughness values, however, this was not the focus of this paper.

Ba Saleem's conclusion that embedment is not a function of clamp length could reasonably be considered true for the clamp lengths tested in this study between 34 and 50 mm. As clamp length decreased the preload loss increased, but the total amount of embedment remained approximately the same.

The total embedment that occurred in steel testing was consistently less then what Ba Saleem predicted in the VDI. This could be attributed to the type of bolts used, the test duration or the clamped material used in Ba Saleem's testing. Ba Saleem stated he used 1045 steel but did not specify if it was hot or cold rolled, and did not specify the material makeup of the bolts used in his experimentation or the length of the dynamic testing completed. If the bolts were stainless steel more preload losses would be expected as stainless-steel experiences more creep, then carbon steel. [6] The time dependent

properties of embedment or creep was much greater in the 6061-T6511 aluminum than the 1045 steel as the aluminum control tests experienced much larger preload losses.

As the material roughness increased so did the initial amount of embedment that occurred in the bolted joint due to external loading. As the external load applied by the UTM increased the amount of embedment that occurred increased as well. As the applied force by the UTM increased the embedment increased. These observations were all consistent with Ba Saleem's.

Ba-Saleem also stated that preload losses slowed down to a negligible degree after three days. The experimental results from this experiment had little bearing this conclusion for testing done with the cold rolled 1045 steel, but the results found for aluminum did not support this conclusion. The time dependent properties of aluminum or the creep in the material proved to be the most influential factor in observing the loss in preload of the joints of aluminum. The test duration of three days should have been extended to better observe the time dependent properties of both the 1045 steel and 6061-T6511 aluminum.

6.0 APPENDIX

6.1 Material Properties

Table 11: VDI 2230 material properties [3]

			Tensile Strength	**Proof Stress @ 0.2%**	**Limiting surface Pressure**	**Young's Modulus**
Material Group	**Material #**	**US Equivalent**	(N/mm^2)	(N/mm^2)	(N/mm^2)	(N/mm^2)
Plain Structural Steels	1.0036	ASTM A283, Grades C,D; ASTM A1011 Gr 33	340	230	490	205000
	1.0050	ASTM A1011, Gr 50; ASTM A572, Gr 50	470	270	710	
	1.0553	ASTM A633, Gr C,D; ASTM A572, Gr 50	490	325	760	
Grain-refined Structural Steels	1.0972	ASTM A1008 / A1011 Gr 45, Class 1,2	390	315	540	205000
	1.0980	ASTM A1008 / A1011 Gr 60, Class 1,2	480	420	670	
Low-alloy tempering steels (heat treated)	1.1192	AISI 1045	700	430	770	205000
	1.5231	No US equivalent	900	600	990	
	1.6582	AISI 4335, AISI 4340	1100	900	1430	
	1.7034	AISI 5135	850	630	1105	
	1.7131	AISI 5115	1000	850	1300	
	1.7225	AISI 4140/4142	1000	750	1300	
	1.7220	AISI 4135	900	650	1170	
Austenitic CrNi Steels	1.4301	ASTM A240 / A276, Type 304	520	210	630	200000
	1.4303	ASTM A240, Type 305	500	220	630	
	1.4307	ASTM A240 / A276, Type 304L	520	200	630	
	1.4401	ASTM A240 / A276, Type 316	530	220	*630*	
	1.4980	ASTM A453 / A630, Grade 660	960	660	1200	211000

Cast Iron	0.6025	ASTM A48, Class 35	250	165[b]	850[c]	110000
	0.7040	ASTM A536, Grade 60-40-18	400	280[b]	600[c]	169000
	0.7050	ASTM A536, Grade 70-50-05	500	350[b]	750[c]	169000
	0.7060	ASTM A536, Grade 100-70-03	600	420[b]	900[c]	174000
	5.2100	ASTM A842, Grade 300	300	210	480	137000
	5.2301	No US equivalent Grade 500	500	350	950	152000
Wrought Aluminum Alloys	3.2315.61	ASTM B221 6082-T6, -T651, -T6511	260	200	325	75000
	3.2315.62	ASTM B221 6082-T6, -T651, -T6511	290	250	360	
	3.3547.08	ASTM B209 / B221 5083-O, -H111, -H112	260	110	325	
	3.4365.71	ASTM B209/B211/B221 7075-T6, -T62, -T651	540	470	*540*	
Cast Aluminum Alloys[1]	3.2163.01	No US equivalent sand casting	160	100	200	75000
	3.2163.62	ASTM B85 380.0-F	180	110	225	
	3.2163.05	ASTM B85 380.0-F	240	140	300	
	3.2371.61	ASTM B26/B108 A356.0-T6, -T61	230	190	290	
	3.2371.62	ASTM B26/B108 A356.0-T6, -T61	250	200	310	70000
	3.2381.01	No US equivalent sand casting	220	180	275	73000
Magnesium Alloys	EN-MC21110	ASTM B94 AZ91A, AZ91B, AZ91D	200	150	280	45000
		ASTM B94 AZ91A, AZ91B, AZ91D; -T4	240	120	290	
	EN-MC21320	ASTM B94 AS41A, AS41B	190	120	230	

6.2 Friction Coefficient Raw Data

Table 12: Aluminum raw slip testing data

	Roughness (Rz) [µm]		
	<15	30	130
Test 1	0.19	0.27	0.36
Test 2	0.19	0.19	0.36
Test 3	0.20	0.26	0.36
Test 4	0.21	0.18	0.33
Test 5	0.21	0.27	0.30
Test 6	0.19	0.18	0.28
Average Slip Coef	0.20	0.22	0.33

Table 13: Steel raw slip testing data

	Roughness (Rz) [µm]		
	<15	30	130
Test 1	0.20	0.21	0.35
Test 2	0.17	0.19	0.35
Test 3	0.16	0.18	0.40
Test 4	0.15	0.20	0.36
Test 5	0.11	0.19	0.38
Test 6	0.17	0.18	0.50
Test 7	0.20	0.18	0.53
Average Slip Coef	0.17	0.19	0.40

6.3 Clamp Length Testing Raw Data

Table 14: Embedment and clamp length testing

Test	Clamp Length	Preload (N)	Preload Loss (N)	Embedment [µm]	Temp change ΔC	Preload Loss (%)
1	1.92	26371	524	3.18	0.29	1.99
2		23971	528	3.20	-0.03	2.20
3		24202	662	4.02	0.12	2.73
1	1.66	22541	818	4.15	0.61	3.63
2		23165	651	3.30	0.22	2.81
3		25257	576	2.92	0.18	2.28
1	1.33	25349	886	3.81	0.34	3.49
2		24332	704	3.02	0.16	2.89
3		24332	704	3.02	0.16	2.89

6.4 Steel Roughness and Embedment Testing

Table 15: 1045 steel embedment testing raw data

Rz [um]	Applied Force [N]	Max Clamp Load [N]	Max embedment [µm]	Temp change [ΔC]	Surface Pressure [Mpa]	Clamp Load Loss [%]
<15	11121	43280	2.94	-0.21	235	1.32
		39719	1.66	-0.28	216	0.81
		40432	1.59	-0.18	220	0.77
		43342	1.32	-0.88	236	0.59
		39537	1.58	0.63	215	0.78
		41081	1.35	0.07	223	0.64
Average		**41232**	**1.74**	**-0.14**	**224**	**0.82**
<15	6672	41500	1.64	0.33	226	0.77
		39719	1.66	-0.28	216	0.81
		40432	1.59	-0.18	220	0.77
		43342	1.32	-0.88	236	0.59
		39537	1.58	0.63	215	0.78
		45490	1.70	0.57	247	0.72
Average		**41670**	**1.58**	**0.03**	**226**	**0.74**
30	11121	40265	4.50	0.08	219	2.17
		41359	3.59	-0.42	225	1.69
		39607	4.13	0.09	215	2.02
		40234	2.64	0.16	219	1.27
		40531	3.00	-0.52	220	1.44
Average		**40399**	**3.57**	**-0.12**	**220**	**1.72**
30	6672	40399	3.57	-0.12	220	1.72
		38632	2.47	0.56	210	1.24
		44906	2.16	0.16	244	0.94
		42765	1.74	0.13	232	0.79
		43228	1.63	-0.21	235	0.73
Average		**41986**	**2.31**	**0.10**	**228**	**1.08**
130	14457	40738	7.99	-0.16	221	3.67
		42046	7.34	-0.51	229	3.26
		40602	10.22	0.28	221	4.70
		47062	12.17	0.56	256	4.64
		46968	9.97	0.24	255	3.81
		47298	8.60	0.68	257	3.31
Average		**44119**	**9.38**	**0.18**	**240**	**3.90**
130	11121	39756	8.08	0.29	216	3.80
		41727	7.10	-0.06	227	3.18
		41409	6.14	0.00	225	2.77
		43798	6.63	0.30	238	3.02
		43871	4.42	2.33	238	2.01
		44456	6.50	0.34	242	2.91
Average		**42503**	**6.48**	**0.53**	**231**	**2.95**
130	6672	48533	7.01	-0.92	264	2.63
		44471	4.24	-0.09	242	1.74
		43251	3.19	0.31	235	1.43
		46592	4.79	0.30	253	2.00
		44650	4.06	0.19	243	1.77
Average		**45499**	**4.66**	**-0.04**	**247**	**1.91**

Table 16: 6061-T6511 Aluminum embedment testing raw data

Rz [um]	Applied Force [N]	Max Force [N]	Max embedment [µm]	Temp change [ΔC]	Surface Pressure [Mpa]	Clamp Load Loss [%]
<15	11121	42659	6.43	0.38	232	4.57
		46953	5.31	0.17	255	1.98
		45259	5.04	0.21	246	1.95
		44194	2.85	-0.01	240	1.12
		45627	3.07	0.09	248	1.18
Average		**44938**	**4.54**	**0.17**	**244**	**2.16**
<15	6672	43978	5.26	-0.22	239	2.09
		39410	2.45	-1.51	214	1.09
		43053	3.23	0.41	234	1.31
		46012	3.14	0.13	250	1.19
		45378	3.78	1.18	247	1.45
		41459	1.99	0.45	225	0.84
Average		**43062**	**2.92**	**0.13**	**234**	**1.18**
30	14457	44690	7.13	-1.03	243	2.94
		41528	5.86	0.38	226	2.60
		45917	9.52	0.33	250	3.71
		45815	11.61	-0.03	249	4.54
		44238	9.24	0.62	240	3.74
Average		**44438**	**8.67**	**0.05**	**242**	**3.51**
30	11121	43148	9.38	0.34	235	3.89
		42391	5.32	-1.59	230	2.25
		46372	6.95	0.01	252	2.68
		43589	7.30	0.59	237	3.09
		43394	5.50	-0.42	236	2.34
Average		**43779**	**6.89**	**-0.21**	**238**	**2.85**
30	6672	43589	7.49	0.59	237	3.09
		39806	4.69	1.05	216	2.12
		42510	4.33	0.42	231	1.83
		39806	4.83	0.81	216	2.12
Average		**41898**	**5.64**	**0.53**	**228**	**2.40**
130	14457	43215	15.77	0.31	235	6.40
		43724	22.92	0.16	238	9.19
		42839	21.89	0.10	233	8.96
		46902	16.54	0.48	255	6.18
Average		**43716**	**16.55**	**0.32**	**238**	**6.63**
130	11121	44300	11.56	1.04	241	4.58
		42636	10.15	0.08	232	4.18
		43877	12.09	0.50	238	4.83
		44134	8.38	0.46	240	3.30
		42574	10.06	-0.11	231	4.11
		41513	12.53	-0.97	226	5.25
Average		**42947**	**10.64**	**-0.01**	**233**	**4.33**
130	6672	37611	4.75	0.51	204	2.20
		39040	5.22	0.20	212	2.33
		39565	4.95	0.98	215	2.18
		42084	6.17	-0.22	229	2.55
		44923	9.06	0.32	244	3.51
Average		43497	7.74	-0.02	236	3.09

7.0 REFERENCES

[1] Blatt. 2003. “Ingenieure Vdi 2230.”

[2] Ba-Saleem, M. O.: Theoretische und experimentelle Untersuchungen der Setzverluste an Schraubenverbindungen. Dissertation Technische Universität Chemnitz, 1991

[3] The Association of German Engineers, 2015, “Systematic Calculation of Highly Stressed Bolted Joints – with One Cylindrical Bolt,” VDI 2230 Part 1

[4] Lori, W.: Beitrag zur Berechnung und Gestaltung von hochfesten Stahlschraubenverbindungen mit keramischen Werkstoffen. Dissertation TH Zwickau, 1989

[5] German Institute for Standardization, 1987, “M1.6 to M39 Hexagon Head Bolts,” DIN 931-1987

[6] Tendo, M.; Takeshita, T.; Nakazawa, T.; Kimura, H.; Abo, H.: Room temperature creep behavior of stainless steels, Tet-su-to-Hagane 79 (1993), 98–104

[7] Schneider, W.: Institut für Werkstoffkunde der TH Darmstadt, unveröffentlicht

[8] Wächter, K.; Beer, R.; Jannasch, D.: Elastische Schraubennachgiebigkeit. Maschinenbautechnik 28 (1979) 3, S. 113–116

[9] Melino, P. (2019). Static Load Bolted Joint Elastic Resilience Testing Methodology.

[10] Lori, W; Gläser, H.: Berechnung der Plattennachgiebigkeit bei Schraubenverbindungen. Konstruktion 42 (1990) 9, S. 271–277

[11] Fritsche, G.: Grundlagen einer genauen Berechnung statisch und dynamisch beanspruchter Schraubenverbindungen. Dissertation TU Berlin, 1962

[12] Nguyen, V. Ph.: Zur genauen Berechnung einer Schraubenverbindung. Forschung im Ingenieurwesen 54 (1988) 1, S. 1–8

[13] Birger, I. A.: Opredelenie podatlivosti promezutocnych detailej rezbovogo soedinenija. Vestnik Mashinostroenija. Moskva 41 (1961) 5, S. 41–44

[14] Lori, W.: Untersuchungen zur Plattennachgiebigkeit in Einschraubverbindungen. Konstruktion 48 (1996) 11, S. 379–382

[15] Lange, H.; Lori, W.: Verbesserte FE-Berechnung der Plattennachgiebigkeit von Einschraubverbindungen. Unveröff. Material des Arbeitsausschusses VDI 2230, 2001

[16] Wiegand, H. ; Illgner, K. H. ; Beelich, K. H.: Über die Verminderung der Vorspannkraft von Schraubenverbindungen durch Setzvorgänge. Werkstatt und Betrieb 98 (1965), S. 823–827

[17] International Standards Organization, 1997, “Geometrical Product Specifications (GPS) — Surface Texture: Profile Method,” ISO 4287-1997

[18] Afzali, N., Pilhagen, J., Manninen, T., Schedin, E., & Stranghöner, N. (2017). Preload losses in stainless steel bolting assemblies. *Steel Construction, 10*(4), 310-318. doi:10.1002/stco.201710041

[19] Pang, X., Hu, Y., Tang, S., Xiang, Z., Wu, G., Xu, T., & Wang, X. (2019). Physical properties of high-strength bolt materials at elevated temperatures. *Results in Physics, 13*, 102156. doi:10.1016/j.rinp.2019.102156

[20] Den Otter, C., & Maljaars, J. (2020). Preload loss of stainless steel bolts in aluminum plated slip resistant connections. *Thin-Walled Structures, 157,* 106984. doi:10.1016/j.tws.2020.106984

[21] 2019, "Bolt Strain Gauge | Tokyo Measuring Instruments Laboratory Co., Ltd.", Tml.jp [Online]. Available: https://tml.jp/e/product/strain_gauge/btm_list.html. [Accessed: 15- Aug- 2019].

[22] Hradil, P., Chen, A., & Baddoo, N. (2017). Numerical modelling of stainless steel preloaded bolted connections. *Steel Construction, 10*(4), 344-353. doi:10.1002/stco.201710039

[23] McGinty, B. (n.d.). Strain gauges. Retrieved March 30, 2021, from http://www.continuummechanics.org/straingauges.html

[24] The effect of Bolted Joint DEFORMATION loss due to embedding. (n.d.). Retrieved February 14, 2021, from https://www.boltscience.com/pages/basics8.htm